PAPER REF: 3944

THE INFLUENCE OF LOCALISED PIT DISTRIBUTION ON THE ULTIMATE STRENGTH OF SHIP STRUCTURAL MEMBERS

Y. Wang[1,2(*)], J.A. Wharton[1], R.A. Shenoi[2]

[1]National Centre of Advanced Tribology at Southampton, Engineering Sciences, University of Southampton, UK
[2]Fluid Structure Interactions Research Group, University of Southampton, UK
[(*)]*Email:* yw5g10@soton.ac.uk

ABSTRACT

Finite element (FE) method is widely used for strength analysis in the shipping industry. This work numerically assesses the influence of corrosion damage on the ultimate strength of steel plates of ship hulls. Corrosion patterns based on American Bureau of Shipping (ABS) pitting diagrams are generated on the strength models. The efficiency of the repair rules issued by Lloyd's Register (LR, 2001) is assessed. A thermoelastic stress analysis (TSA) test is utilised to validate the FE models.

Keywords: modelling, ultimate strength, pitting corrosion, degree of pitting, thermoelastic stress analysis.

INTRODUCTION

The worldwide fleet of ships is ageing, with many vessels being over 15 years old. For such vessels, corrosion is an ongoing concern and indeed recently a severe corrosion situation termed 'super-rust', with corrosion rates of up to 5 mm per year, has been observed within the ullage space of oil cargo holds (Howarth & Dawson, 2012). This ultimately poses significant maintenance problems and increases the risk to structural integrity, potentially leading to loss of cargo, pollution to the environment and danger to life. Thus, to guarantee structural integrity, facilitate maintenance decisions economically, and even extend the structural life, it is becoming essential to investigate the ultimate strength of such aged and corroded ships based on a more comprehensive understanding of the corrosion mechanisms. Both experimental and numerical work has been conducted to assess the ultimate strength reduction of corroded structural members (mostly steel plates) (Paik et al., 2003; Nakai et al., 2004a, 2004b; Mobesher & Sumi, 2010 and Ruwan et al., 2011), focusing on various loading conditions (uniaxial compressive / tensile pressure, shear force along edges and pure bending moment), material properties (nonlinear stress-strain relationship), structural properties (aspect ratio, slenderness ratio and initial geometric imperfection) and corrosion features (volume loss, degree of pitting (DOP), pit shape and depth and pit locations).

The recently issued pitting diagram (ABS, 2007) indicates that there is a need to investigate the influence of more localised areas of corrosion on the structural strength. In terms of the experimental work, strain gauges have been widely used at discrete locations over the specimen surface. However, due to the geometric non-linearity of the corrosion patterns, the stress change of high gradient around the defects is of equal or even greater importance, since the stress concentration could in future lead to an accelerated corrosion rate. To date, only FE modelling has provided this information, however there is no full field measurement currently available in the published literature. In addition, there are no reported validations of the stress distribution from numerical modelling.

This paper presents a full-field measurement provided by TSA carried out as a validation of the models. Furthermore, a series of FE models focusing on the influence of the location of one-side corrosion on steel plates by considering geometric and material nonlinearities is included. Four corrosion patterns are applied to the modelling. Additionally, plates without corrosion are tested for comparison and calibration of the experimental results.

TSA VALIDATION

As a non-contacting technique TSA is able to provide full-field stress data over the surface of a cyclically loaded specimen within the elastic region of the material (Dulieu-Barton & Stanley, 1998). A basic first-order relationship between the principle stress change and the temperature change forms the foundation of the TSA technique. For an isotropic material the following expression has been established,

$$\Delta T = -KT\Delta(\sigma_1 + \sigma_2) \tag{1}$$

where K is the thermoelastic constant of the material, $K = \alpha/(\rho C_p)$, α is the coefficient of thermal expansion, ρ is the density of the material, C_p is the specific heat at a constant pressure, T is the absolute temperature of the specimen surface and $\Delta(\sigma_1 + \sigma_2)$ is the sum of the principle surface stresses. Equation (1) is valid when (Dulieu-Barton & Stanley, 1998):

i) The material behaviour is elastic;
ii) The relevant material properties such as Young's modulus are not temperature dependent;
iii) The temperature change in the material is under an adiabatic condition.

Using a servo-hydraulic test machine, the cyclic loading ensures an adiabatic thermal condition, for which the surface temperature change associated with the stress change was monitored by a Cedip 480M infrared detector. A thin matt black paint of 15 – 25 μm in thickness, as suggested in (Robinson et al., 2010), was applied on the test area to achieve a uniform high emissivity for which the radiant energy can be measured quantitatively.

The specimens were fabricated from EN3B steel plate, with a density of 7870 kg m^{-3}, a Young's modulus of 188 GPa, Poisson's ratio of 0.3 with the yield stress of 520 MPa. Fig. 1(a) illustrates an example of the artificial corroded specimen. The dimension of the test area was 90 × 90 × 3 mm. Three artificial circular defects were randomly distributed on the surface with various remaining thickness (0.33t, 0.5t and t), where t is the original plate thickness. The DOP is 5% and the total volume loss is 582.5 mm^3. Both top and bottom edges of the specimen were bolted to jigs, which were gripped by the test machine, as shown in Fig. 1(b). A sinusoidal load waveform with amplitude of 20 $\pm$ 15 kN was utilised by keeping the upper jaw fixed and lower jaw moving up and down at a frequency of 5Hz. TSA tests were conducted on both sides per specimen. The rate of data capture of the Cedip system was defined as 383Hz for a 320 × 256 pixel field of view. Calibration was achieved by testing an intact specimen under the same loading conditions. Since pure tensile loading leads to $\sigma_2 = 0$, the thermoelastic constant K was calculated using Equation (1) by knowing the cross-sectional area, input load, specimen surface temperature and detected maximum temperature change.

Finite element models of the test specimens are built in ANSYS14.0, considering both quadratic shell and solid (reduced integration) elements. Convergence studies are carried out to determine the optimum mesh shape and mesh size. Mapped mesh with triangular-

/tetrahedral-shaped elements is applied. The loading and boundary conditions are kept the same as those for the TSA tests.

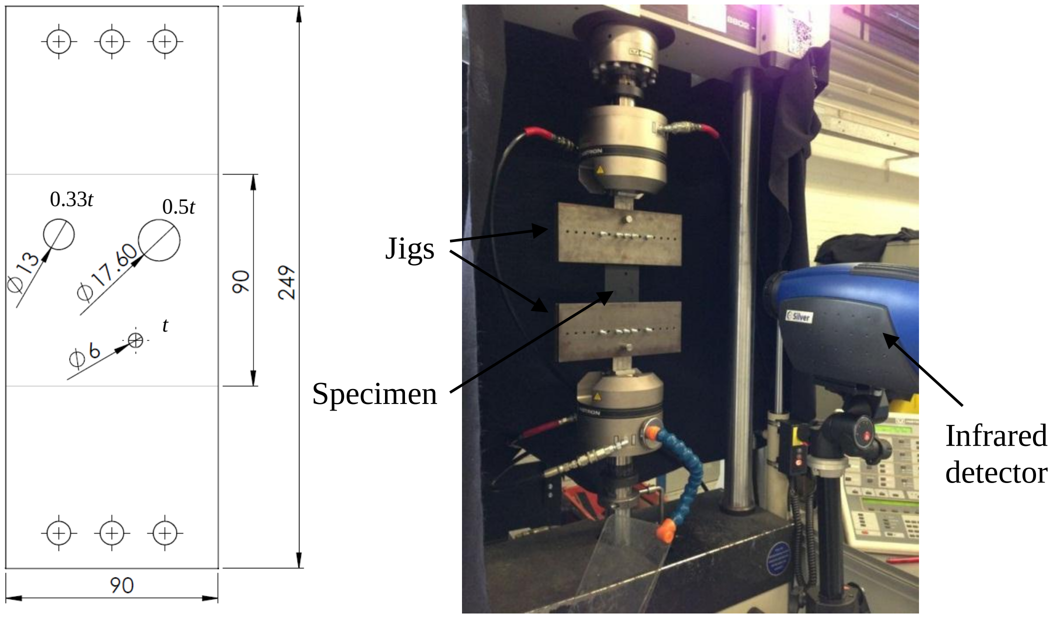

(a) (b)

Fig. 1 TSA specimen sketch with dimensions in millimetres (a) and experimental set-up (b)

VALIDATION AND DISCUSSION

An example of the calibrated principle stress distributions on both sides of the specimen are shown in Figs. 2 and 3, with the results from the numerical modelling. It can be seen that TSA successfully detected the stress concentrations around the artificial pit defects and the interactions between them on both surfaces of the specimen. The comparisons of the stress contours indicate a good correlation between the numerical and experimental results. The maximum principle stress occurs along the edge of the hole, as expected. To further demonstrate the quality of the numerical model, line data at y = 66 mm are obtained from TSA and FE results and plotted in Fig. 4. Good agreement between TSA and numerical results can be found with minor variations.

The main source of error is considered to be the difference in the spatial resolution of TSA and FE models and the uniformity of the paint thickness. Specifically, the line data from the FE model were derived by interpolation of the nodal stresses. The distance between two interpolation points is 0.18 mm, while the distance between two pixels in TSA is 0.352 mm. This difference may be a main contribution to the error especially at the areas with rapidly changing geometry. In addition, it is difficult to guarantee a uniform thickness of the paint around the edges of the defects. This variation may reduce the emissivity, and hence the quality of the experimental data.

The overall good agreement between experimental and numerical data provides greater reassurance in the adoption of FE technique for further strength analyses in consideration of different, more complex corrosion patterns and loading conditions.

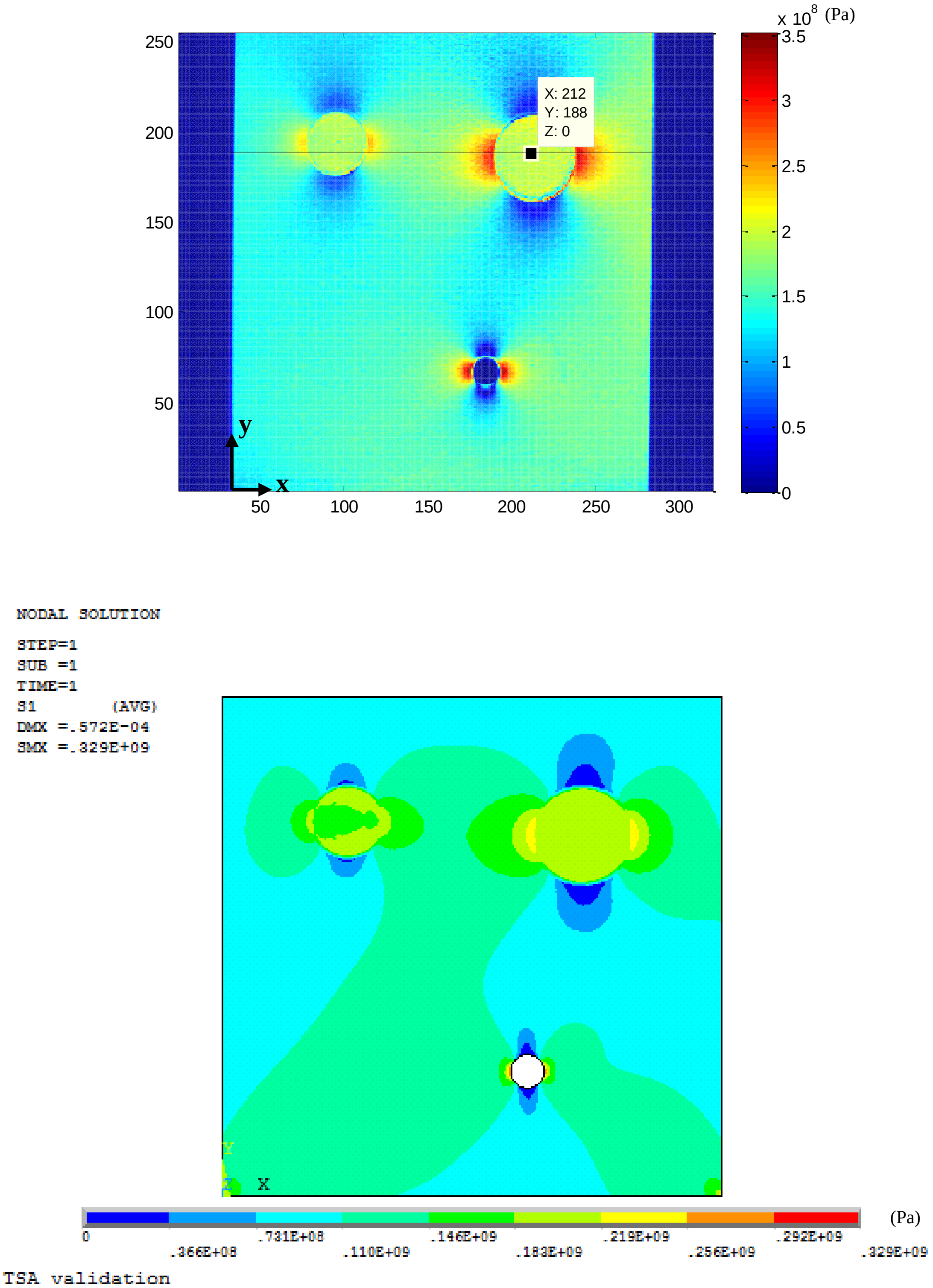

Fig. 2 Principle stress distributions on the front of the specimen (top: TSA; bot: FE model)

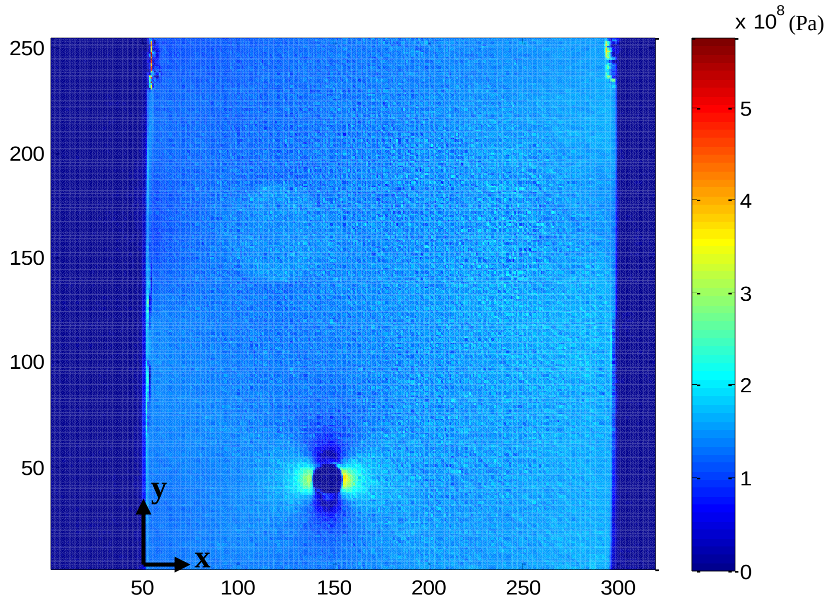

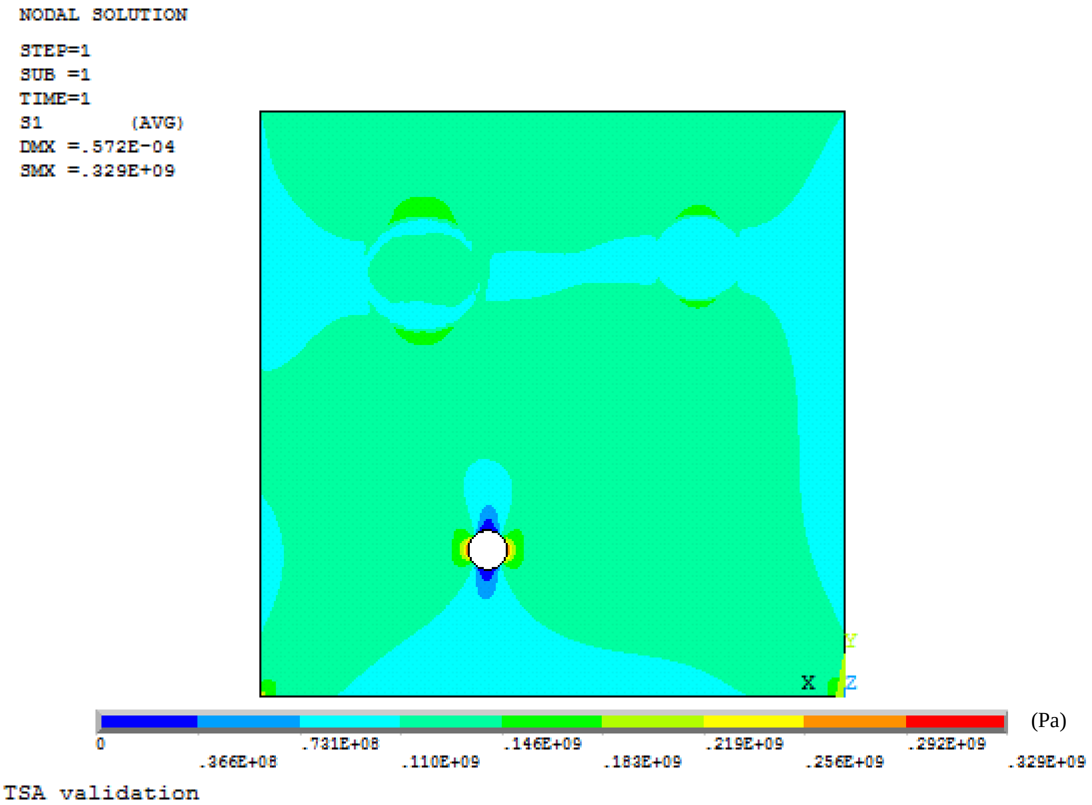

Fig. 3 Principle stress distributions on the back of the specimen (top: TSA; bot: FE model)

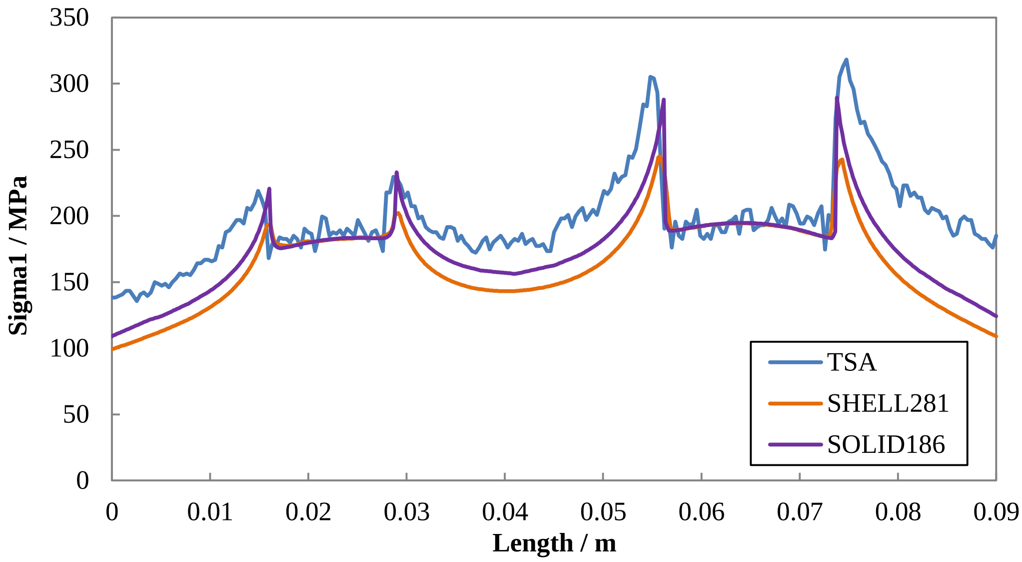

Fig. 4 Principle stress distributions on the back of the specimen (top: TSA; bot: FE model)

ULTIMATE STRENGTH ANALYSIS

The ultimate strength analysis was achieved using an FE methodology by considering geometric and material nonlinearities. ANSYS 14.0 was used for the large deflection static analysis. Both shell and solid elements were adopted to construct the models. The novel modelling approach focuses on the influence of the location of one-side corrosion on steel plates of a size 800 × 800 × 15 mm. The test matrix, was based on the repair methods issued by LR (2001), contains five DOP (2%, 5%, 10%, 15% and 25%) and four thickness reduction values (0.25*t*, 0.33*t*, 0.5*t* and 0.75*t*), where *t* is the original plate thickness. The ABS pitting intensity diagrams (2007) were also utilised in the generation of the four corrosion patterns (Fig. 5).

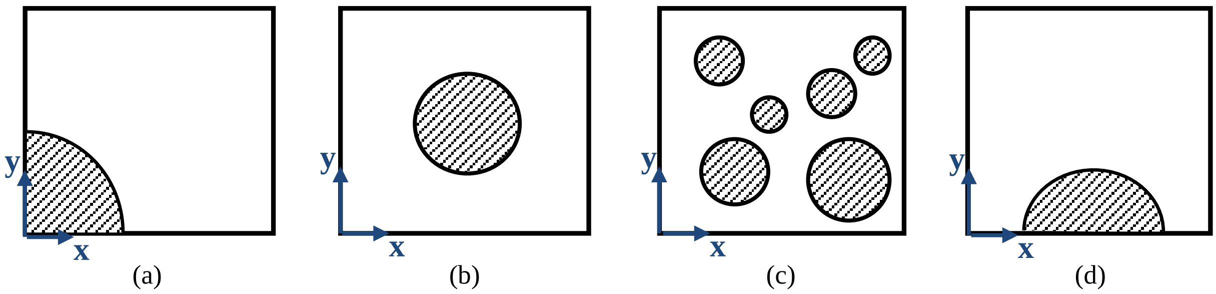

Fig. 5 Studied corrosion patterns: (a) corrosion at the corner; (b) corrosion in the centre; (c) random pitting; (d) corrosion at the unloaded edges

All plates were simply supported along four edges and under uniaxial compressive loading in the x direction. Geometric imperfection $w = 0.1\beta^2 t \sin(\pi x/a) \sin(\pi y/a)$ was introduced to the models, where β is the slenderness ratio and a is the length of the plate. Plates were loaded until and after the ultimate strength state was reached.

RESULTS AND DISCUSSION

The axial compressive strength values of the plates were derived for every substep and plotted against the strain value in order to determine the ultimate strength and to quantify the strength behaviour. The normalised results of ultimate strength reduction and ultimate strain values are plotted against the different DOP and pit depth, as shown in Fig. 6.

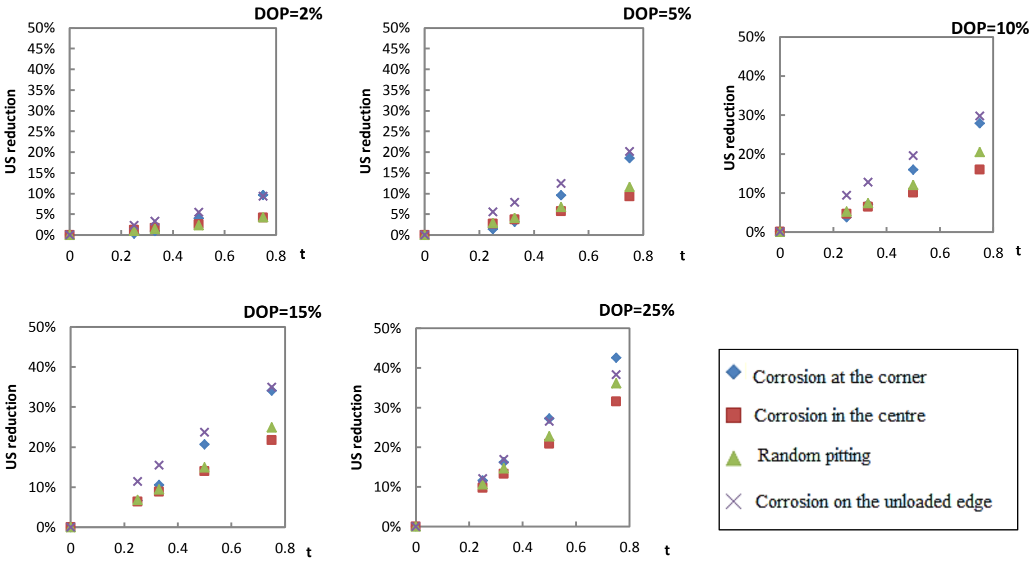

Fig. 6 Ultimate strength reduction for square steel plates

The numerical modelling findings are as follows:

- The strength values decrease when increasing DOP or the corrosion depth, as expected;
- The difference in the strength reduction between central and random pitting corrosion patterns is fairly small;
- According to the ABS rules, when DOP exceeds 15%, the corrosion condition needs to be checked during the ship survey. The results show when DOP is equal to 15% the ultimate strength reduction can range from 6.4% to 34.9%;
- LR rules indicate that an epoxy filling is needed when corrosion depths exceed 0.33*t*, while welding is necessary when corrosion depth is beyond 0.5*t* and DOP is more than 25%. Based on the results, the strength reduction for 0.33*t* ranges from 0.88% to 16.89%, while the reduction for the latter condition varies from 20.86% to 27.25%. There is no clear differentiation between these two ranges;
- Higher ultimate strength reduction is found when corrosion occurs at the left corner or on the unloaded edge.

CONCLUSIONS

This paper shows a validation of the FE modelling against experimental data considering artificial corrosion patterns on steel plates. A full-field measurement technique, TSA, was used to validate the stress distribution over the plate surface. Using the validated element type and meshing method, ultimate strength analyses were conducted numerically, focusing on the effect of the corrosion locations. This initial study demonstrates the importance to introduce more realistic corrosion patterns to the strength modelling. Further experimental and numerical studies will be performed that consider real corroded surfaces and welding effects.

ACKNOWLEDGMENTS

The authors gratefully acknowledge the funding by the University of Southampton and The Lloyd's Register Educational Trust University Technology Centre (The LRET UTC).

REFERENCES

American Bureau of Shipping (2007). Guidance notes on the inspection, maintenance and application of marine coating systems. Available online: http://www.eagle.org/eagleExternalPortalWEB/appmanager/absEagle/absEagleDesktop?_nfpb=true&_pageLabel=abs_eagle_portal_rules_guides_download_page&pub_id=49 (Access date: 11/03/2013)

Dulieu-Barton, J.M. and Stanley, P. (1998). "Development and applications of thermoelastic stress analysis." The Journal of Strain Analysis for Engineering Design **33**(2): 93-104.

Howarth, D and Dawson, R (2012). Personal communication, Lloyd's Register, London, UK.

LR (2001). Lloyd's Register Guidance Information - Naval survey guidance for steel ships.

Mobesher Ahmmad, M. and Sumi, Y. (2010). "Strength and deformability of corroded steel plates under quasi-static tensile load." Journal of Marine Science and Technology **15**: 1-15.

Nakai, T., Matsushita, H. and Yamamoto, N. (2004b). "Effect of pitting corrosion on local strength of hold frames of bulk carriers (2nd report) - Lateral-distortional buckling and local face buckling." Marine Structures **17**: 612-641.

Nakai, T., Matsushita, H., Yamamoto, N. and Arai, H. (2004a). "Effect of pitting corrosion on local strength of hold frames of bulk carriers (1st report)." Marine Structures **17**: 403-432.

Paik, J.K., Lee, J.M. and Ko, M.J. (2003). Ultimate compressive strength of plate elements with pit corrosion wastage Proceedings of the Institution of Mechanical Engineers. **217:** 185-200.

Robinson, A.F., Dulieu-Barton, J.M., Quinn, S. and Burguete, R.L. (2010). "Paint coating characterization for thermoelastic stress analysis of metallic materials." Measurement Science and Technology **21**: 1-11.

Ruwan S. Appuhamy, J.M., Ohga, M., Kaita, T. and Dissanayake, R. (2011). "Reduction of ultimate strength due to corrosion - A finite element computational method." International Journal of Engineering **5**(2): 194-207.